Available online at www.sciencedirect.com
ScienceDirect
Journal of the European Ceramic Society 29 (2009) 525–535
www.elsevier.com/locate/jeurceramsoc

Mechanical properties of Hi-Nicalon fiber-reinforced celsian composites after high-temperature exposures in air

Narottam P. Bansal *

Structures and Materials Division, NASA Glenn Research Center, Cleveland, OH 44135, USA

Received 21 April 2008; received in revised form 13 June 2008; accepted 19 June 2008
Available online 26 July 2008

Abstract

BN/SiC-coated Hi-Nicalon fiber-reinforced celsian matrix composites (CMCs) were annealed for 100 h in air at various temperatures to 1200 °C, followed by flexural strength measurements at room temperature. Values of yield stress and strain, ultimate strength, and composite modulus remain almost unchanged for samples annealed up to 1100 °C. A thin porous layer formed on the surface of the 1100 °C annealed sample and its density decreased from 3.09 to 2.90 g/cm^3. The specimen annealed at 1200 °C gained 0.43% weight, was severely deformed, and was covered with a porous layer of thick shiny glaze which could be easily peeled off. Some gas bubbles were also present on the surface. This surface layer consisted of elongated crystals of monoclinic celsian and some amorphous phase(s). The fibers in this surface ply of the CMC had broken into small pieces. The fiber–matrix interface strength was characterized through fiber push-in technique. Values of debond stress, σ_d, and frictional sliding stress, τ_f, for the as-fabricated CMC were 0.31 ± 0.14 GPa and 10.4 ± 3.1 MPa, respectively. These values compared with 0.53 ± 0.47 GPa and 8.33 ± 1.72 MPa for the fibers in the interior of the 1200 °C annealed sample, indicating hardly any change in fiber–matrix interface strength. The effects of thermal aging on microstructure were investigated using scanning electron microscopy. Only the surface ply of the 1200 °C annealed specimens had degraded from oxidation whereas the bulk interior part of the CMC was unaffected. A mechanism is proposed explaining the various steps involved during the degradation of the CMC on annealing in air at 1200 °C.
Published by Elsevier Ltd.

Keywords: Ceramic composites; Mechanical properties; SiC fibers; Barium aluminosilicate; Fiber–matrix interface

1. Introduction

Fiber-reinforced ceramic matrix composites (CMCs) are prospective candidate materials for high-temperature structural applications in various industries such as aerospace, power generation, energy conservation, nuclear, petrochemical, and transportation. A number of ceramic and glass–ceramic composite systems[1,2] are being developed in various research laboratories. Barium aluminosilicate with monoclinic celsian phase is one of the most refractory glass–ceramics. It has a melting point of >1700 °C, is phase stable to ~1600 °C, and is oxidation resistant. Over the last few years, at NASA Glenn Research Center, celsian matrix composites[3–9] reinforced with silicon carbide-based fibers have been investigated for use in hot sections of turbine engines. Results for Nicalon and Hi-Nicalon fiber-reinforced celsian matrix composites have been reported earlier.[6–17] During high-temperature use, CMC components are prone to degradation in their mechanical properties due to oxidation. Tensile, flexural, and shear properties, at temperatures up to 1200 °C in air, have been reported for celsian matrix composites reinforced with Nicalon[6] as well as Hi-Nicalon[12,14,16] fibers. However, no information is available about the influence of long-term high-temperature exposures on the mechanical properties of these CMCs. The primary objective of this study was to investigate the effects of high-temperature annealing in oxidizing environment on the mechanical properties and microstructural stability of Hi-Nicalon fiber-reinforced celsian matrix composites. The room temperature strength of the composites, after annealing in air at various temperatures from 550 to 1200 °C, was measured in three-point flexure. The fiber–matrix interface strength was analyzed using a fiber push-in technique.[15]

* Tel.: +1 216 433 3855.
E-mail address: narottam.p.bansal@nasa.gov.

0955-2219/$ – see front matter. Published by Elsevier Ltd.
doi:10.1016/j.jeurceramsoc.2008.06.023

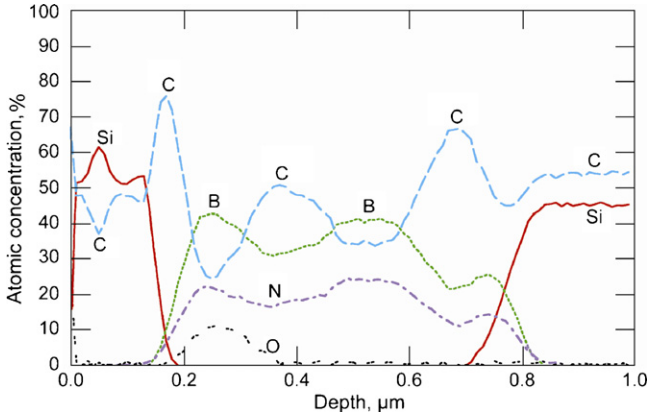

Fig. 1. Scanning Auger microprobe depth profiles of various elements for Hi-Nicalon fibers having a duplex "BN/SiC" surface coating deposited by CVD.

2. Materials and experimental methods

Polymer derived Hi-Nicalon fiber tows (1800 denier, 500 filaments/tow) with low oxygen content from Nippon Carbon Co. were used as the reinforcement.[18,19] A duplex surface layer of boron nitride (BN) over coated with silicon carbide was applied on the fibers by a commercial vendor using a continuous chemical vapor deposition (CVD) reactor. The BN coating was deposited at ~1000 °C utilizing a proprietary precursor and was amorphous to partly turbostratic in nature. A thin overcoating of SiC was also deposited by CVD onto the BN-coated fibers. The SiC layer was crystalline. The nominal coating thicknesses were 0.4 μm for BN, and 0.3 μm for SiC. The BN interfacial layer was intended to be a weak, crack deflecting phase, while the SiC overcoat was used as a barrier to diffusion of boron from BN into the oxide matrix and also prevents diffusion of matrix elements into the fiber. The matrix of $0.75BaO–0.25SrO–Al_2O_3–2SiO_2$ (BSAS) composition was synthesized by a solid-state reaction method as described earlier.[20] The advantage of BSAS over BAS as matrix has been explained earlier.[11,20] Briefly speaking, hexacelsian is the first phase to form in both BAS and SAS systems. On heat treatment at ~1200 °C or higher temperatures, transformation of hexacelsian to monoclinic celsian phase is very sluggish in BAS and very rapid in SAS.[8] However, it is known that substitution of about 25 mol% of BaO with SrO in BAS accelerates the transformation[23] of hexacelsian to the desired monoclinic celsian phase.

The experimental setup and the procedure used for fabrication of the fiber-reinforced celsian matrix CMC were essentially the same as described earlier.[10,11] The matrix precursor powder was made into a slurry by dispersing in an organic solvent along with organic additives as binder, surfactant, deflocculant and plasticizer followed by ball milling. Tows of BN/SiC-coated Hi-Nicalon fibers were coated with the matrix precursor by passing through the slurry and winding on a rotating drum. After drying, the prepreg tape was cut to size. Unidirectional fiber-reinforced composites were prepared by tape lay-up (12 plies) followed by warm pressing to form a "green" composite. The fugitive organics were slowly burned out of the sample in air, followed by hot pressing under vacuum in a graphite die to yield dense composites. The oxide precursor was converted into the desired monoclinic celsian phase *in situ* during hot pressing as was confirmed from X-ray diffraction. The hot pressed CMC panel ~11.1 cm × 5 cm (4.5 in. × 2 in.) was annealed in argon at 1100 °C for 2 h and machined into test bars (~50 mm × 0.625 mm × 2.4 mm) for high-temperature

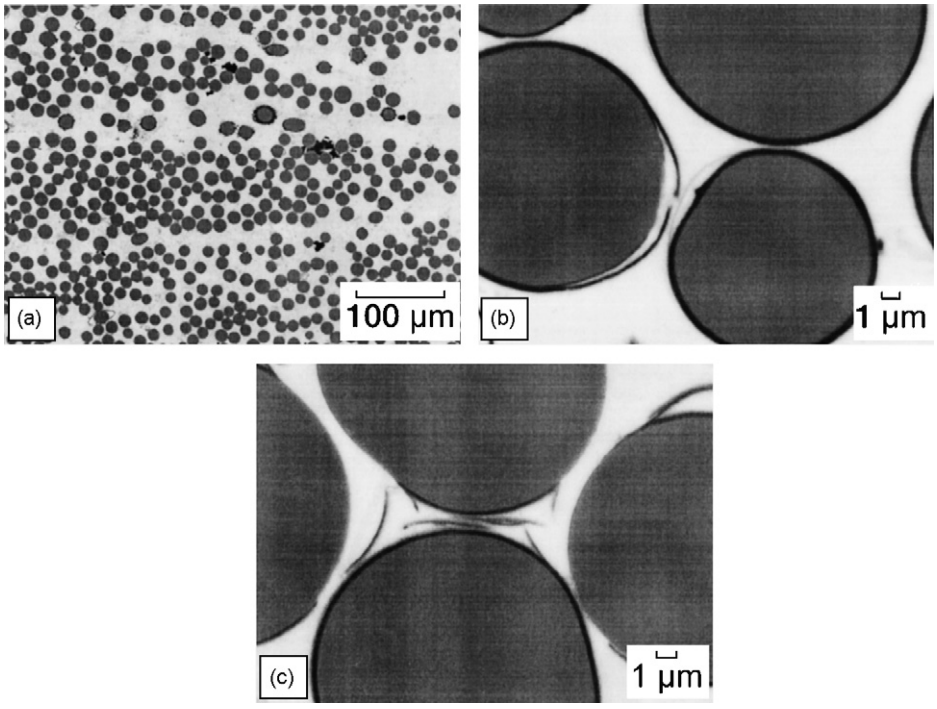

Fig. 2. SEM micrographs at different magnifications showing polished cross-section of a unidirectional Hi-Nicalon/BN/SiC/BSAS composite.

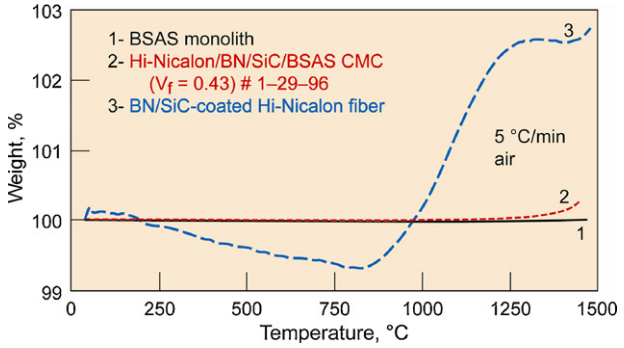

Fig. 3. TGA curves for BSAS monolith, BN/SiC-coated Hi-Nicalon fiber and Hi-Nicalon/BN/SiC/BSAS composite recorded at a heating rate of 5 °C/min in air.

exposures in air and mechanical testing. The volume fraction of fibers in the composite was found to be ~0.32.

For high-temperature annealing, the CMC bars were rested on the edges of an alumina boat placed inside a programmable box furnace. The furnace temperature was raised at a heating rate of 20 °C/min. CMC bars were annealed at 550, 800, 900, 1000, 1100, and 1200 °C for 100 h in stagnant ambient air and furnace cooled. Dimensions and weight of each test bar were recorded before and after annealing.

Mechanical properties were determined from apparent stress–strain curves recorded from a three-point flexure test using an Instron 4505 universal testing machine at a cross-head speed of 1.27 mm/min (0.05 in./min) and support span (L) of 40 mm. Strain gauges were glued to the tensile surfaces of the flexure test bars. Stress, σ, was calculated from beam theory, assuming a linear elastic beam, using the equation:

$$\sigma = \left[\frac{3PL}{2bh^2}\right] \quad (1)$$

where b and h are the width and thickness of the test sample and P is the load. The yield stress, σ_y, was taken from the onset of deviation from linearity in the stress–strain curve. Elastic modulus of the composite was determined from the linear portion of the stress–strain curve.

Cyclic fiber push-in tests were performed using a desktop apparatus previously described,[21] but with the addition of a symmetrically placed pair of capacitance gauges for displacement measurements. Thin sections of the composites, cut normal to the fiber axis with a diamond saw, and polished down to a 0.1-μm finish on both top and bottom faces were tested. Final specimen thickness was typically about 3 mm. Fibers were pushed in using a 70°-included-angle conical diamond indenter with a 10-μm diameter flat base. To prevent the sides of the conical indenter from impacting the matrix, push-in distances were restricted to just a couple of microns. Unless otherwise noted, each test consisted of five cycles of loading and unloading between a selected maximum load and a minimum load of 0.01 N at room temperature in ambient atmosphere.

Thermogravimetric analysis (TGA) was carried out at a heating rate of 5 °C/min under flowing air from room temperature to 1500 °C using a PerkinElmer TGA-7 system, which was interfaced with a computerized data acquisition and analysis system. X-ray diffraction (XRD) patterns were recorded at room temperature using a step scan procedure (0.02°/2θ step, time/step 0.5 or 1 s) on a Phillips ADP-3600 automated diffractometer equipped with a crystal monochromator employing Cu Kα radiation. Density was measured from dimensions and mass as well as by the Archimedes method. Microstructures of the polished cross-sections and fracture surfaces were observed in a JEOL JSM-840A scanning electron microscope. Prior to analysis, a thin layer of carbon was evaporated onto the SEM specimens for electrical conductivity.

The elemental compositions of the fiber surface coatings were analyzed with a scanning Auger microprobe (Fisons Instruments Microlab Model 310-F). The fibers for this analysis were mounted on a stainless steel sample mount by tacking the ends with colloidal graphite. Depth profiling was performed by sequential ion-beam sputtering and Auger analysis. The ion etching was done with 3 keV argon ions rastered over an approximately 1 mm^2 area. The etch rate in Ta_2O_5 under these conditions was 0.05 nm/s. Auger electron spectroscopy (AES) analysis of the coated Hi-Nicalon fibers was performed using an electron beam current of approximately 1.5 nA. The beam was rastered over a 2 μm × 20 μm area of the fiber with the long axis of the area aligned with the long fiber axis. Spectra were acquired in integral mode at beam energy of 2 keV and depth profiles were generated by plotting elemental peak areas against ion etch time. The atomic concentrations were calculated by dividing the peak areas by the spectrometer transmission function and the sensitivity factors for each peak, then scaling the results to total 100%. The sensitivity factors were derived from spectra of ion etched Si, B, SiC, BN, and TiO_2 standards. The depth scale is from the Ta_2O_5 calibration and no attempt has been made to adjust for the actual etch rate for each material. Only the fibers with a smooth surface coating, rather than those having thick and rough coating morphologies, were used for Auger analysis.

3. Results and discussion

3.1. Scanning Auger analysis

Elemental composition depth profiles obtained from scanning Auger microprobe analysis for the BN/SiC coatings on Hi-Nicalon fibers are shown in Fig. 1. The coating consists of ~0.15 μm thick Si-rich SiC followed by ~0.6 μm of carbon rich "BN". In addition, unintentionally deposited carbon layer is also present between the SiC and "BN" coatings. Another predominantly carbon layer is also seen between the "BN" coating and the fiber surface. Presence of free Si has also been detected[13] in the SiC coating layer by Raman microspectroscopy. This is consistent with the results of another study[22] which found the SiC layer to be rich in Si from scanning Auger analysis.

3.2. Microstructural analysis

SEM micrographs taken from the polished cross-section of the unidirectional hot pressed composite are shown in Fig. 2.

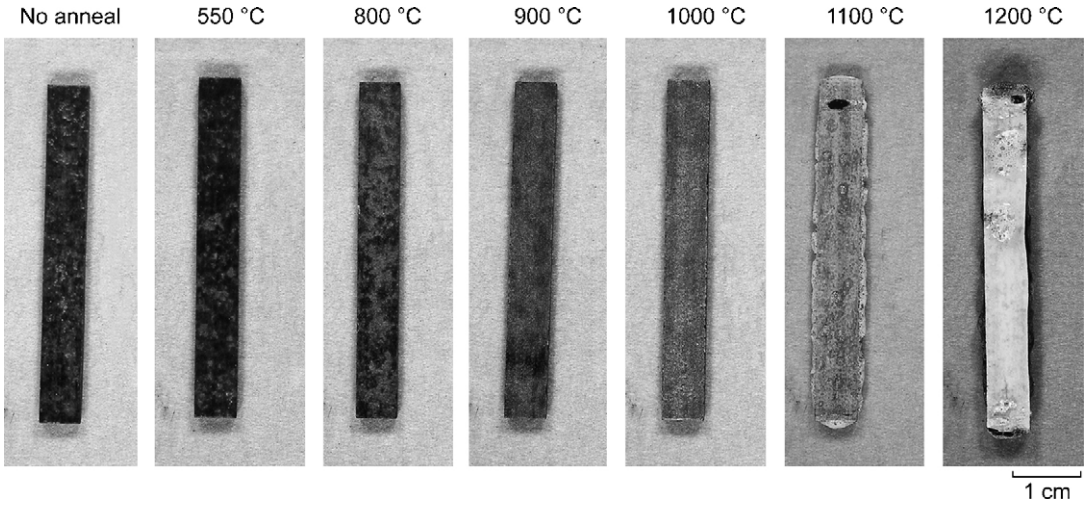

Fig. 4. Optical photographs showing Hi-Nicalon/BN/SiC/BSAS composite bars annealed for 100 h in air at various temperatures.

Uniform fiber distribution and good matrix infiltration within the fiber tows are evident. Some matrix porosity is also present. Some of the filaments are of irregular shape rather than having circular cross-section. The manufacturer reports an average fiber diameter of ∼14 μm, but a large variation in the diameter of the filaments within a fiber tow can be seen. The BN/SiC surface coating has been detached from some of the fibers during metallography or composite processing. Debonding or loss of the fiber coating may lead to adverse reactions between the fibers and the oxide matrix at high-temperature resulting in strong fiber–matrix bonding.

3.3. Thermogravimetric analysis

The TGA curve for the Hi-Nicalon/BN/SiC/BSAS composite with a fiber volume fraction of 0.43 is given in Fig. 3. Also shown for comparison are the curves for the BN/SiC-coated Hi-Nicalon fibers and a BSAS monolithic sample hot pressed at 1300 °C for 2 h at 4 ksi (∼27.6 MPa). The monolithic ceramic exhibits hardly any weight change and appears to be stable up to 1500 °C in air. The composite shows a negligible weight change up to ∼1150 °C. The total weight gain at 1450 °C is also small (∼0.3%). In contrast, the fibers initially loose ∼0.5% weight

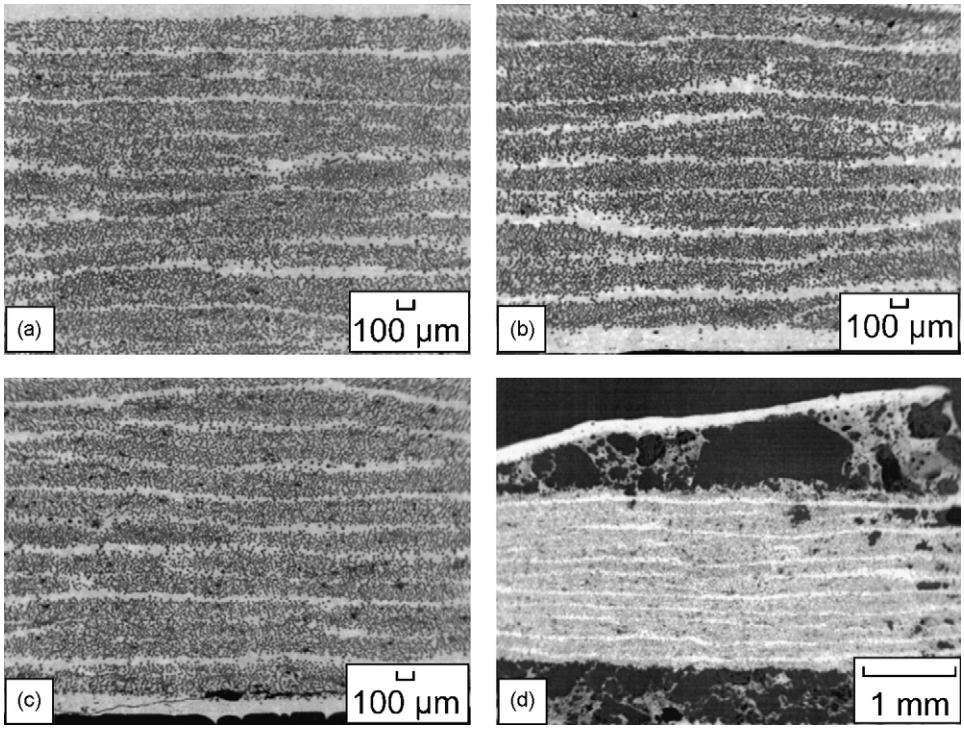

Fig. 5. SEM micrographs of polished cross-sections of unidirectional Hi-Nicalon/BN/SiC/BSAS composites annealed in air for 100 h at various temperatures: (a) as-fabricated, (b) 1000 °C, (c) 1100 °C, and (d) 1200 °C.

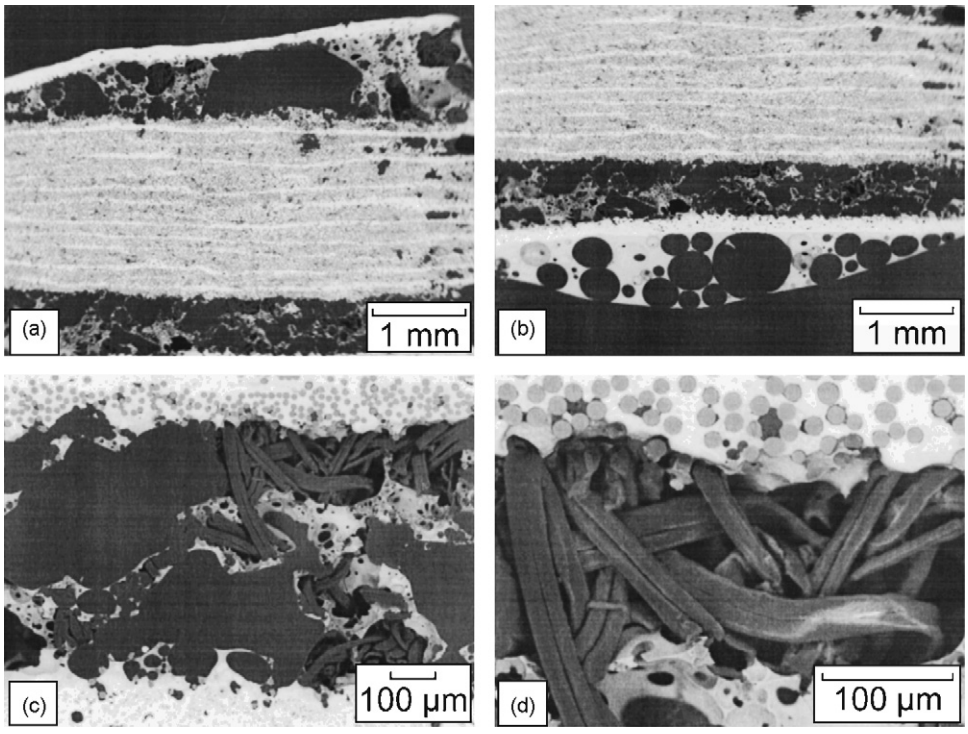

Fig. 6. SEM micrographs of polished cross-sections of unidirectional Hi-Nicalon/BN/SiC/BSAS composites annealed at 1200 °C for 100 h in air.

up to ~850 °C, probably due to the loss of absorbed moisture. This is followed by a large weight increase, possibly due to the oxidation of BN into B_2O_3 and also SiC to SiO_2, particularly at higher temperatures. The total weight gain is found to be ~3%.

3.4. Thermal ageing in air

CMC bars were heat treated in ambient air for 100 h at various temperatures. Optical photographs showing the physical appearance of the CMC bars before and after annealing at various temperatures are shown in Fig. 4. No changes in physical appearance were observed in samples annealed at 1000 °C or lower. However, the specimen annealed at 1100 °C was covered with a thin porous white layer that could be easily removed by polishing with a fine emery paper. The samples aged at 1200 °C were deformed and developed a thick shiny white layer on the exposed surfaces. Pores were present in the surface layer. Signs of partial melting and gas bubble formation during heat treatment were also observed. From XRD analysis, both amorphous and celsian phases were detected in the surface layer. Since such a behavior was not observed[23] in monolithic BSAS material even after heat treatment for 20 h in air at 1500 °C, it is assumed to be caused by the presence of Hi-Nicalon fibers and the BN/SiC coating. In the presence of air, BN is probably oxidized to B_2O_3 which reacts with the matrix and/or silica formed from the oxi-

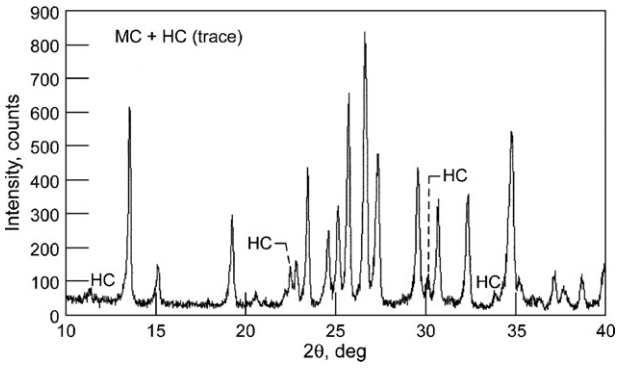

Fig. 7. X-ray diffraction pattern taken from the surface of as hot-pressed. Hi-Nicalon/BN/SiC/BSAS composite. MC: monoclinic celsian; HC: hexacelsian.

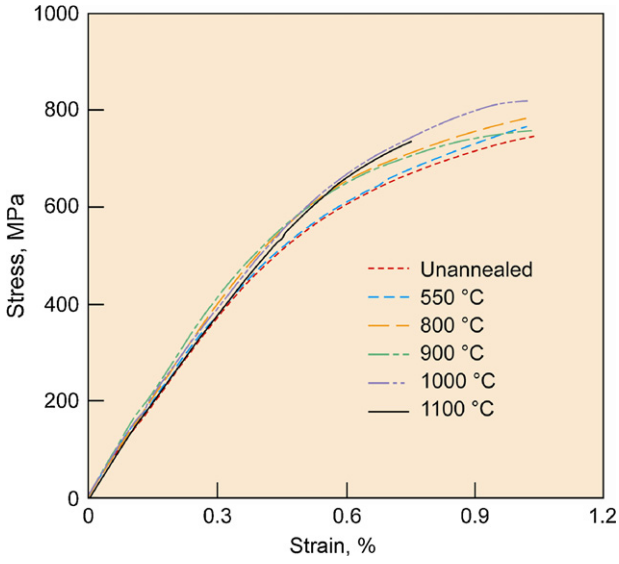

Fig. 8. Apparent stress–strain curves recorded in three-point flexure for BN/SiC-coated Hi-Nicalon fiber-reinforced celsian matrix composites annealed in air for 100 h at various temperatures. (For interpretation of the references to color in the artwork, the reader is referred to the web version of the article.)

Table 1
Mechanical properties[a] of unidirectional Hi-Nicalon/BN/SiC/BSAS composite annealed at various temperatures for 100 h in air; $V_f = 0.32$ (#Hi-NIC-BSAS-6-24-97)

Annealing temperature (°C)	Density (g/cm^3)	Weight change after annealing	E_c (GPa)	σ_y (MPa)	ε_y (%)	σ_u (MPa)
–	3.09 ± 0.03	–	137	122	0.091	759
550	3.12	None	145	155	0.108	853
800	3.06	None	150	138	0.096	814
900	3.16	None	151	171	0.114	769
1000	3.04	None	146	134	0.092	819
1100	2.90	None	142	143	0.102	736
1200	Deformed	+0.43%				

[a] Measured at room temperature in three-point flexure.

dation of silicon carbide fibers, resulting in low-melting glassy phase which migrates to the sample surface. The bubble formation may be related to the oxidation of Hi-Nicalon fibers producing amorphous silica and volatile CO and CO_2 gases.

Stability of BN in moisture and oxygen containing atmospheres is an intrinsic problem in the long-term use of this material as fiber–matrix interface.[24] At 700 °C, the sensitivity to moisture is controlled by the crystalline structure. Also, formation of boric acid is minimal below 800 °C. However, B_2O_3 reacts readily with water to form HBO_2. Therefore, in the presence of moisture, B_2O_3 will undergo significant weight loss. The product of hydrolysis is predominantly metaboric acid (HBO_2) with traces of orthoboric acid (H_3BO_3). In dry air, BN shows minimal oxidation up to 800 °C. At higher temperatures, B_2O_3 glass is formed on its surface. B_2O_3 has a low vapor pressure ($<2 \times 10^{-3}$ Torr) and volatilizes slowly at temperatures less than 1100 °C. Most of the BN coatings on fibers are deposited at relatively low temperatures (~1000 °C) and generally are contaminated with carbon and oxygen impurities. Also, these BN coatings consist of randomly oriented microcrystalline or turbostratic grains and lack well ordered microstructures. The stability of BN towards moisture and its resistance towards air oxidation depend on the degree of its crystallinity.[24] BN with large d (0 0 2) spacing is much more reactive towards moisture than those close to the hexagonal BN structure probably because of its less densely packed basal planes implying weaker atomic bonding. The higher the value of d (0 0 2) interlayer spacing, the less crystalline the material. BN with an interlayer spacing of d (0 0 2) = 0.335 nm (3.35 Å), which is close to the theoretical value of 0.333 nm, showed significantly improved stability towards moisture and air.

The matrix layers on the surface of CMC specimens annealed at 1100 and 1200 °C appear to have cracked and delaminated, respectively as seen in the SEM micrographs (Fig. 5) taken from the polished cross-sections. A large difference in the coefficients of thermal expansion (CTE) of Hi-Nicalon fiber (~3.5×10^{-6} °C^{-1}) and the oxide matrix[20] (~5.28×10^{-6} °C^{-1}) may be responsible for the observed cracking and delamination. This would provide an easy path for the ingression of oxygen to the fiber bundles and accelerate the degradation of fibers from oxidation. No such cracking or delamination was observed in samples annealed at lower temperatures. Higher magnification SEM micrographs (Fig. 6) from the 1200 °C annealed specimens show the presence of gas bubbles on its surface. Severe damage is also observed underneath the top debonded layer where damaged broken pieces of the fibers are also present.

3.5. X-ray diffraction analysis

XRD pattern recorded from surface of the as-fabricated CMC panel is given in Fig. 7. It shows the presence of only monoclinic celsian along with a trace amount of hexacelsian. Additional diffraction peaks at d values of 0.504 nm ($2\theta = 17.5°$) and 0.312 nm ($2\theta = 28.5°$) were detected in samples annealed at 900, 1000, and 1100 °C. The peak at $d = 0.312$ nm was much stronger than the one at $d = 0.504$ nm in the 900 °C annealed specimen where as the reverse was true for the CMC annealed at 1000 and 1100 °C. The phase corresponding to these peaks could not be identified. A white shiny and glassy layer was formed on the surface of the sample annealed at 1200 °C. The surface layer was found to contain monoclinic celsian and an unidentified amorphous phase from XRD analysis.

3.6. Mechanical properties

Apparent stress–strain curves recorded in three-point flexure for the unidirectional BSAS matrix composite reinforced with BN/SiC-coated Hi-Nicalon fibers, before and after thermal aging in air at various temperatures to 1100 °C, are presented in Fig. 8. In earlier studies[11,20] hot pressed BSAS monolithic material showed flexural strength of 130 MPa, elastic modulus of 96 GPa, and failed in a brittle mode, as expected. In contrast, the composites show initial linear elastic behavior followed by an extended region of load carrying capability beyond the initial deviation from linearity. This indicates load transfer to the fibers beyond the proportional limit indicating graceful failure and true composite behavior. Various room temperature mechanical properties of the composites, before and after thermal aging in air at various temperatures, are summarized in Table 1. The measured elastic modulus of the CMC is in good agreement with a value of 150 GPa, calculated from the rule-of-mixtures ($E_c = V_m E_m + V_f E_f$ where V is the volume fraction and the subscripts c, m, and f refer to the composite, matrix, and fiber, respectively) using $E_m = 96$ GPa[20] and $E_f = 270$ GPa.[18,19] There is no effect of thermal annealing in air up to 1100 °C on the values of elastic modulus, yield stress, yield strain, and ultimate stress of the composites. Mechanical behavior of the CMC annealed at 1200 °C could not be recorded as this specimen had badly deformed.

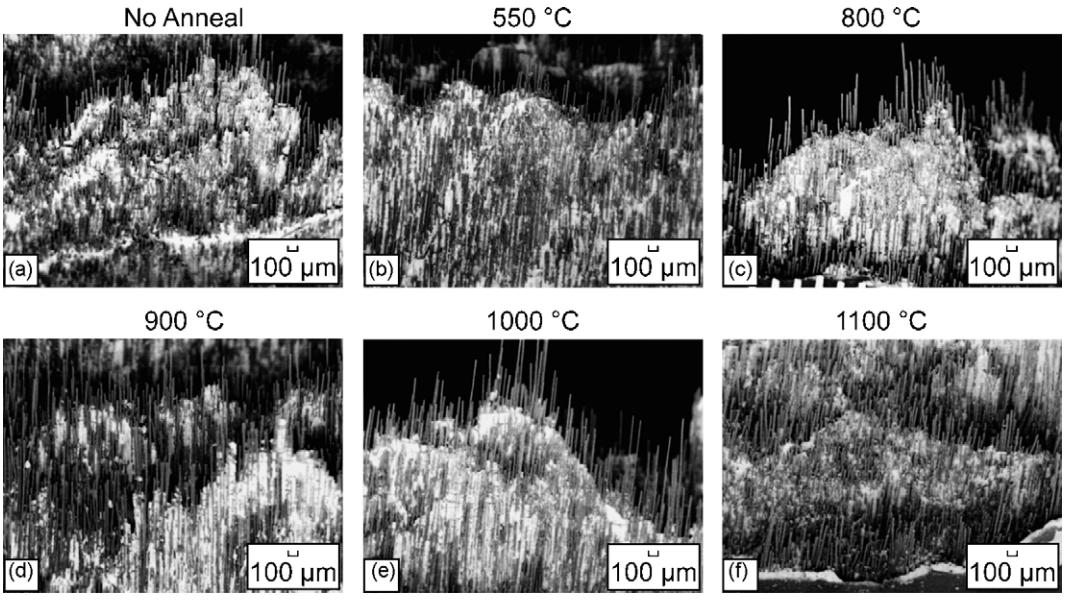

Fig. 9. SEM micrographs showing fracture surfaces of BN/SiC-coated Hi-Nicalon fiber-reinforced celsian matrix composites annealed in air for 100 h at various temperatures.

3.7. SEM of fracture surfaces

SEM micrographs of fracture surfaces of the composites, annealed for 100 h in air at various temperatures up to 1100 °C, after the room temperature flexure test, are shown in Fig. 9. Extensive long lengths of fiber pullout are observed indicating toughening behavior for all the annealed CMC samples. Typical higher magnification SEM pictures showing fracture surfaces of the as-fabricated CMC and the one air-annealed at 1100 °C are presented in Fig. 10. Debonding occurs primarily between the fiber and the innermost coating in both specimens. In some instances, the coating appears to stay with the fibers, particu-

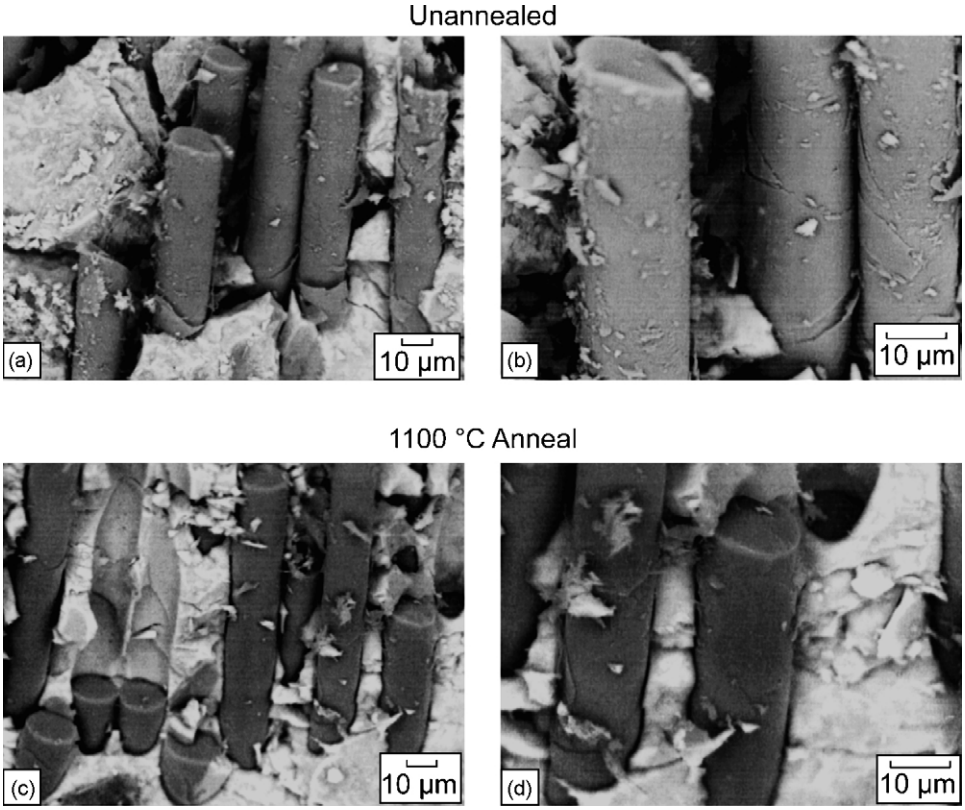

Fig. 10. SEM micrographs showing fracture surfaces of BN/SiC-coated Hi-Nicalon fiber-reinforced celsian matrix composites: as-fabricated and those annealed at 1100 °C for 100 h in air.

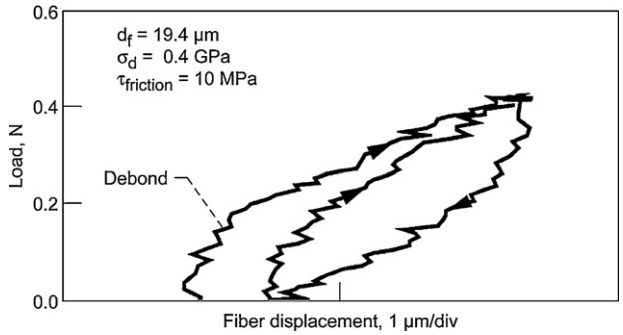

Fig. 11. Load versus fiber displacement curve recorded during fiber push-in test of as-fabricated celsian matrix composite reinforced with BN/SiC-coated Hi-Nicalon fibers.

larly in the unannealed sample. Surface of the debonded fibers appears to be smooth indicating no fiber degradation or chemical reaction with the matrix during high-temperature annealing at 1100 °C.

3.8. Fiber–matrix interface

In as-fabricated fiber-reinforced composites, the fibers may experience a several hundred MPa clamping force upon cooling from the CMC processing temperature. Thermal mismatch stresses result from smaller thermal expansion of reinforcing fibers as compared to the matrix. A compliant layer is necessary to reduce the stresses. The importance of a compliant interface layer for a strong and tough CMC has been emphasized by various workers.[26–29] Both graphitic and pyrolytic carbon and hexagonal or turbostratic BN have exceptionally low moduli. Ceramic composites that demonstrate good damage tolerance generally contain carbon or BN layer between the fiber and matrix with some exceptions such as porous oxide matrix CMCs.

For strong and particularly tough CMCs, the fiber–matrix interface must be sufficiently weak to allow debonding at the interface, yet strong enough for effective load transfer from the matrix to the fiber. Fiber–matrix debonding and frictional sliding stresses at the fiber–matrix interface were evaluated from fiber push-in tests. About 12–15 fibers/coupon were individually pushed in for the air annealed and as-fabricated composites. A typical cyclic push-in curve at room temperature for the as-received composite, along with reloading part of the second cycle, is given in Fig. 11. The data were analyzed by first subtracting the appropriate load-train compliance correction from the measured displacements. An estimate of frictional sliding stress, $\tau_{friction}$, was obtained using the constant $\tau_{friction}$ model of Marshall and Oliver[25] which includes effects of residual stresses, but does not consider fiber roughness or Poisson expansion. Value of $\tau_{friction}$ was determined by fitting the compliance corrected data from each reloading curve to the relationship

$$u = u_0 + \left[\frac{F^2}{8\pi^2 r_f^3 E_f \tau_{friction}}\right] \quad (2)$$

where u is the fiber end displacement, u_0 is the residual fiber end displacement after the previous unloading, F is the applied load, r_f is the fiber radius, and E_f is the fiber modulus. While neglecting Poisson expansion of the fibers leads to an overestimation of $\tau_{friction}$ values, the relative changes in $\tau_{friction}$ with load cycling could be followed using Eq. (2). In addition, a debond initiation stress, σ_d, could be calculated from the debond initiation load, F_d (load at which fiber end begins to move during first loading cycle) by the relation

$$\sigma_d = \frac{F_d}{\pi r_f^2} \quad (3)$$

The results of fiber push-in data are summarized in Table 2. The scatters in the values of debond stress (σ_d) and frictional sliding stress (τ_f) are due to the accuracy of measurements for a particular fiber as well as from the variations in values from fiber-to-fiber. The variation in frictional sliding stress (τ_f) during successive loading–unloading cycles was small and within the standard deviation. Values of debond stress, σ_d, and frictional sliding stress, τ_f, for the as-fabricated CMC were 0.31 ± 0.14 GPa and 10.4 ± 3.1 MPa, respectively, compared with 0.53 ± 0.47 GPa and 8.33 ± 1.72 MPa for the fibers in the interior of the 1200 °C annealed sample. These results indicate that only the outer ply of the 1200 °C annealed CMC specimens has been degraded from oxidation whereas the bulk interior part remains unaffected.

Table 2
Effects of annealing on fiber push-in test results for unidirectional Hi-Nicalon/BN/SiC/BSAS composite; 12 plies, $V_f = 0.32$ (#Hi-NIC-BSAS-6-24-97)

Annealing conditions	σ_d (GPa)	$\tau_{friction}$ (MPa)
As-fabricated	0.31 ± 0.14	10.4 ± 3.1
100 h, air, 1200 °C	0.53 ± 0.47[a]	8.33 ± 1.72[a]

[a] Measured for fibers in the interior of the annealed CMC sample.

3.9. Degradation mechanism at 1200 °C

A possible mechanism explaining the various steps involved in the degradation of Hi-Nicalon/BN/SiC/BSAS CMC on annealing in air at 1200 °C is presented in Fig. 12. During annealing at 1200 °C, the surface matrix layer delaminates from the composite ply underneath (SEM micrograph of Fig. 5), probably due to the large CTE mismatch between the Hi-Nicalon fibers and the celsian matrix. This facilitates the ingression of oxygen into the composite. This causes the oxidation of SiC fibers, particularly those which have lost the duplex CVD coating (see Fig. 2), resulting in the formation of SiO_2:

$$SiC\,(s) + O_2\,(g) \rightarrow SiO_2\,(s) + CO\,(g) + CO_2\,(g) \quad (4)$$

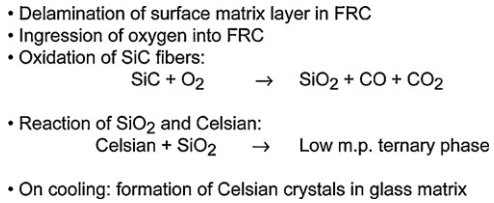

Fig. 12. Proposed mechanism for degradation of Hi-Nicalon/BN/SiC/BSAS composites during annealing at 1200 °C in air.

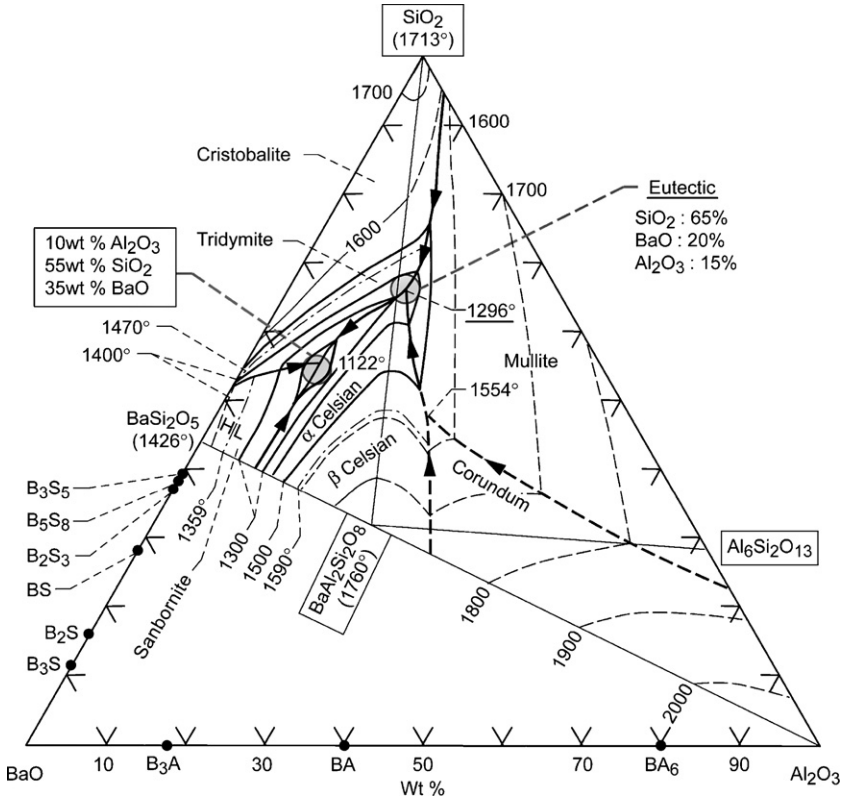

Fig. 13. Phase diagram of $BaO–Al_2O_3–SiO_2$ system showing the presence of low-melting ternary eutectics.

The silica formed reacts with celsian resulting in the formation of a low-melting phase. The phase diagram of $BaO–Al_2O_3–SiO_2$ ternary system[30] is given in Fig. 13. It does show the presence of a ternary phase with a melting point of 1122 °C. This phase is richer in SiO_2 but poorer in BaO and Al_2O_3 than celsian. Formation of gaseous by-products CO and CO_2 during reaction (4) results in the evolution of bubbles as observed in SEM micrograph of Fig. 6. On cooling, celsian crystals precipitate from the melt leaving behind a glassy matrix which is richer in SiO_2 and poorer in BaO and Al_2O_3 than celsian. SEM micrograph (Fig. 14) taken from the surface of 1200 °C annealed CMC shows the presence of elongated crystals in some glassy matrix. From qualitative EDS analysis, these crystals are seen to be celsian and the glassy matrix is found to be richer

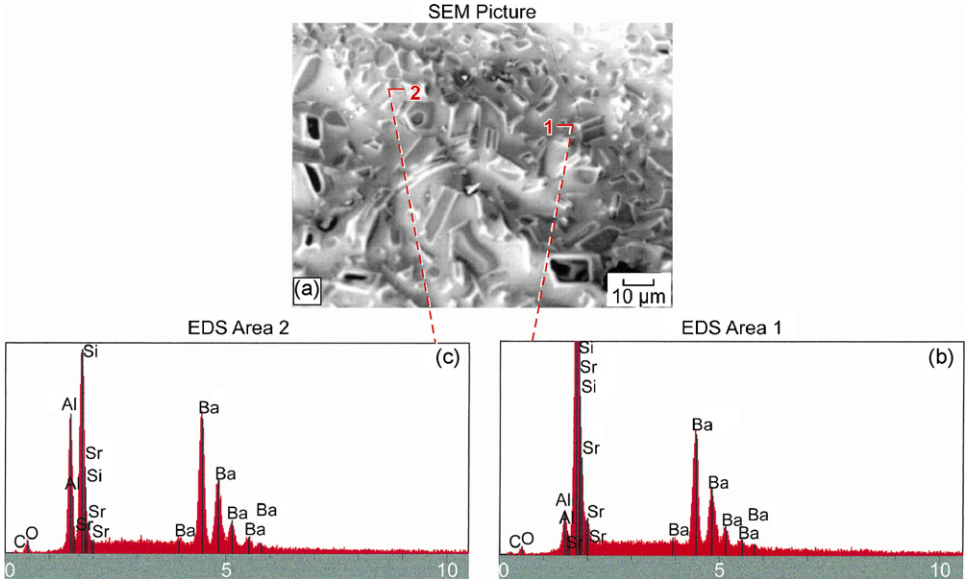

Fig. 14. SEM micrograph showing surface of Hi-Nicalon/BN/SiC/BSAS composite annealed at 1200 °C for 100 h in air. Also shown are the EDS analyses of two different areas, labeled as 1 and 2, of the CMC surface.

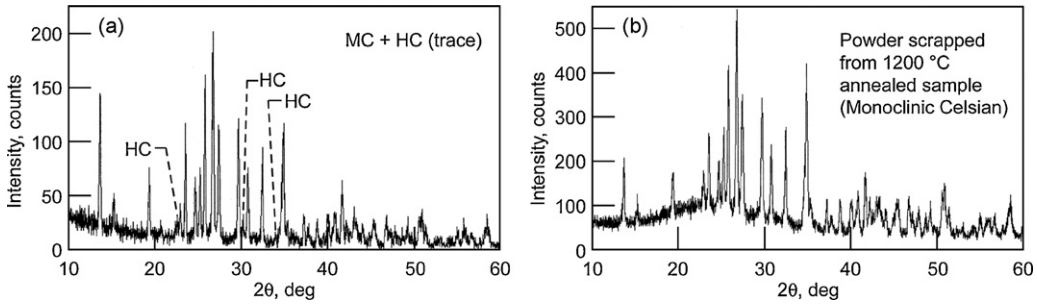

Fig. 15. X-ray diffraction spectra from surfaces of Hi-Nicalon/BN/SiC/BSAS composites: (a) as-fabricated and (b) annealed at 1200 °C for 100 h in air.

in SiO_2 but poorer in BaO and Al_2O_3 than celsian. The XRD patterns taken from the as-fabricated CMC and that annealed for 100 h in air at 1200 °C are given in Fig. 15. Only celsian phase is detected in the as-fabricated sample whereas celsian and some amorphous phase are present in the 1200 °C-annealed CMC. Formation of a low-melting glass phase has also been reported[31] earlier during the study of BSAS environmental barrier coating (EBC) on Si-based ceramic substrates such as CVD SiC and SiC_f/SiC composite. On heat treatment, the plasma sprayed BSAS coating reacted with the silica layer, formed from oxidation of the Si-based ceramic substrate, resulting in low-melting ternary glass phase which was found to be richer in SiO_2 but poorer in BaO and Al_2O_3 than celsian. Formation of amorphous silica, due to the oxidation of SiC whiskers, has also been reported during oxidation study of SiC whisker reinforced mullite/zirconia composites[32] at 1000–1350 °C. At 1200 °C or higher temperatures, formation of zircon was observed from the reaction between ZrO_2 and SiO_2. Secondary mullite grains were also formed through a solution-reprecipitation mechanism.

4. Summary

Room temperature mechanical properties of BN/SiC-coated Hi-Nicalon fiber-reinforced celsian matrix composites remained unaffected after thermal aging for 100 h in air at various temperatures up to 1100 °C. A thin white layer had formed on the surface of the 1100 °C annealed sample and its density decreased from 3.09 to 2.90 g/cm^3. However, the specimen annealed at 1200 °C gained 0.43% weight, deformed in shape and size, and was covered with a thick shiny white porous layer that could be easily peeled off. From X-ray diffraction analysis, this surface layer was found to consist of amorphous and monoclinic celsian phases. The fibers in this surface layer had broken into small pieces. The fiber–matrix interface in the interior of the coupons was characterized through fiber push-in technique. Values of debond stress, σ_d, and frictional sliding stress, τ_f, for the as-fabricated CMC were 0.31 ± 0.14 GPa and 10.4 ± 3.1 MPa, respectively, compared with 0.53 ± 0.47 GPa and 8.33 ± 1.72 MPa for the fibers in the interior of the 1200 °C annealed sample indicating hardly any change in fiber–matrix interface. Microstructures of the annealed specimens were investigated using SEM. Only the surface ply of the 1200 °C annealed specimens had degraded from oxidation whereas the bulk interior part of the CMC was unaffected.

5. Conclusions

Celsian matrix composites reinforced with BN/SiC-coated Hi-Nicalon fibers are stable in air up to 1100 °C. However, their mechanical properties are severely degraded at higher temperatures due to oxidation.

Acknowledgments

Thanks are due to John Setlock, Ron Phillips, Terry Kacik, and Ralph Garlick for their technical assistance during composite processing and characterization. Don Wheeler assisted with the scanning Auger analysis and Jeff Eldridge with fiber push-in testing. This research was supported by NASA's Ultra Efficient Engine Technology (UEET) Project and Hypersonic Project of the Fundamental Aeronautics Program.

References

1. Bansal, N. P., ed., *Handbook of Ceramic Composites*. Kluwer Academic Publishers, Boston (MA), 2005.
2. Boccaccini, A. R., Continuous fiber reinforced glass and glass–ceramic matrix composites. In *Handbook of Ceramic Composites*, ed. N. P. Bansal. Kluwer Academic Publishers, Boston (MA), 2005, pp. 461–484.
3. Bansal, N. P., Ceramic fiber-reinforced glass–ceramic matrix composite. US Patent 5,214,004, May 25, 1993.
4. Bansal, N. P., Method of producing a ceramic fiber-reinforced glass–ceramic matrix composite. US Patent 5,281,559, January 25, 1994.
5. Bansal, N. P., CVD SiC fiber-reinforced barium aluminosilicate glass–ceramic matrix composites. *Mater. Sci. Eng. A*, 1996, **220**(1–2), 129–139.
6. Bansal, N. P., McCluskey, P., Linsey, G., Murphy, D. and Levan, G., Nicalon fiber-reinforced celsian glass–ceramic matrix composites. In *Proceedings of Annual HITEMP Review, Vol. III*, 1995, NASA CP 10178, p. 41-1–14.
7. Bansal, N. P., SiC fiber-reinforced celsian composites. In *Handbook of Ceramic Composites*, ed. N. P. Bansal. Kluwer Academic Publishers, Boston (MA), 2005, pp. 227–249.
8. Bansal, N. P. and Drummond III, C. H., Kinetics of hexacelsian-to-celsian phase transformation in $SrAl_2Si_2O_8$. *J. Am. Ceram. Soc.*, 1993, **76**(5), 1321–1324.
9. Bansal, N. P., Mechanical behavior of silicon carbide fiber-reinforced strontium aluminosilicate glass–ceramic composites. *Mater. Sci. Eng. A*, 1997, **231**(1–2), 117–127.
10. Bansal, N. P. and Setlock, J. A., Fabrication of fiber-reinforced celsian matrix composites. *Composites: Part A*, 2001, **32**, 1021–1029.
11. Bansal, N. P., Strong and tough Hi-Nicalon fiber-reinforced celsian matrix composites. *J. Am. Ceram. Soc.*, 1997, **80**(9), 2407–2409.
12. Gyekenyesi, J. Z. and Bansal, N. P. High temperature mechanical properties of Hi-Nicalon fiber-reinforced celsian composites. In *Advances in Ceramic*

Matrix Composites V, ed. N. P. Bansal, J. P. Singh, and E. Ustundag. Am. Ceram. Soc., Westerville (OH); *Ceram. Trans.*, 2000, **103**, 291–306.
13. Gouadec, G., Colomban, Ph. and Bansal, N. P., Raman study of Hi-Nicalon fiber-reinforced celsian composites. I. Distribution and nanostructure of different phases. *J. Am. Ceram. Soc.*, 2001, **84**(5), 1129–1135.
14. Ünal, Ö. and Bansal, N. P., In-plane and interlaminar shear strength of silicon carbide fiber-reinforced celsian composite. *Ceram. Int.*, 2002, **28**(5), 527–540.
15. Bansal, N. P. and Eldridge, J. I., Hi-Nicalon fiber-reinforced celsian matrix composites: influence of interface modification. *J. Mater. Res.*, 1998, **13**(6), 1530–1537.
16. Choi, S. R. and Bansal, N. P., Shear strength as a function of test rate in SiC_f/BSAS ceramic matrix composite at elevated temperature. *J. Am. Ceram. Soc.*, 2004, **87**(10), 1912–1918.
17. Choi, S. R., Bansal, N. P. and Verrilli, M. J., Delayed failure of ceramic matrix composites in tension at elevated temperature. *J. Eur. Ceram. Soc.*, 2005, **25**(9), 1629–1636.
18. DiCarlo, J. A. and Yun, H. M., Non-oxide (silicon carbide) fibers. In *Handbook of Ceramic Composites*, ed. N. P. Bansal. Kluwer Academic Publishers, Boston (MA), 2005, pp. 33–52.
19. Takeda, M., Sakamoto, J., Saeki, S., Imai, Y. and Ichikawa, H., High performance silicon carbide fiber Hi-Nicalon for ceramic matrix composites. *Ceram. Eng. Sci. Proc.*, 1995, **16**(4), 37–44.
20. Bansal, N. P., Solid state synthesis and properties of monoclinic celsian. *J. Mater. Sci.*, 1998, **33**(19), 4711–4715.
21. Eldridge, J. I. Desktop fiber push-out apparatus. NASA Technical Memorandum 105341, 1991.
22. Bansal, N. P. and Chen, Y. L., Chemical, mechanical and microstructural characterization of low-oxygen containing silicon carbide fibers with ceramic coatings. *J. Mater. Sci.*, 1998, **33**(22), 5277–5289.
23. Bansal, N. P., Hyatt, M. J. and Drummond III, C. H., Crystallization and properties of Sr–Ba aluminosilicate glass–ceramic matrices. *Ceram. Eng. Sci. Proc.*, 1991, **12**(7–8), 1222–1234.
24. Cofer, C. G. and Economy, J., Oxidative and hydrolytic stability of boron nitride–a new approach to improving the oxidation resistance of carbonaceous structures. *Carbon*, 1995, **33**(4), 389–395.
25. Marshall, D. B. and Oliver, W. C., Measurement of interfacial mechanical properties in fiber-reinforced ceramic composites. *J. Am. Ceram. Soc.*, 1987, **70**(8), 542–548.
26. Besmann, T. M., Stinton, D. P., Kupp, E. R., Shanmugham, S. and Liaw, P. K., Fiber–matrix interfaces in ceramic composites. *Mater. Res. Symp. Proc.*, 1997, **458**, 147–159.
27. Hsueh, C. H., Becher, P. F. and Angelini, P., Effects of interfacial films on thermal stresses in whisker reinforced ceramics. *J. Am. Ceram. Soc.*, 1988, **71**(11), 929–933.
28. Kerans, R. J., The role of coating compliance and fiber/matrix interfacial topography on debonding in ceramic composites. *Scr. Metall. Mater.*, 1995, **32**(4), 505–509.
29. Kerans, R. J., Issues in the control of fiber–matrix interface properties in ceramic composites. *Scr. Metall. Mater.*, 1994, **31**(8), 1079–1084.
30. Levin, E. M. and McMurdie, H. F., *Phase Diagram for Ceramists*, *Vol. III*. The Am. Ceram. Soc, Westerville (OH), 1975 [Fig. 4544, p. 220].
31. Lee, K. N., Fox, D. S., Eldridge, J. I., Zhu, D., Robinson, R. C., Bansal, N. P. *et al.*, Upper temperature limit of environmental barrier coating based on mullite and BSAS. *J. Am. Ceram. Soc.*, 2003, **86**(8), 1299–1306.
32. Ruh, R., Mullite-SiC whisker and mullite/ZrO_2–SiC whisker composites. In *Handbook of Ceramic Composites*, ed. N. P. Bansal. Kluwer Academic Publishers, Boston (MA), 2005, pp. 325–346.